Mode-matching for Optical Antennas - Supplementary Material

Thorsten Feichtner
Helmholtz-Zentrum Berlin für Materialien und Energie GmbH, Institut Nanoarchitekturen für die Energieumwandlung, Hahn-Meitner-Platz 1, 14109 Berlin, Germany
Max Planck Institute for the Science of Light - Photonic Nanostructures, Günther-Scharowsky-Strasse 1, Bau 26, 91058 Erlangen, Germany and
Nano-Optics & Biophotonics Group, Department of Experimental Physics 5, Röntgen Research Center for Complex Material Research (RCCM), Physics Institute, University of Würzburg, Am Hubland, D-97074 Würzburg, Germany

Silke Christiansen
Helmholtz-Zentrum Berlin für Materialien und Energie GmbH, Institut Nanoarchitekturen für die Energieumwandlung, Hahn-Meitner-Platz 1, 14109 Berlin, Germany
Max Planck Institute for the Science of Light - Photonic Nanostructures, Günther-Scharowsky-Strasse 1, Bau 26, 91058 Erlangen, Germany and
Freie Universität Berlin, Arnimallee 14, 14195 Berlin

Bert Hecht
Nano-Optics & Biophotonics Group, Department of Experimental Physics 5, Röntgen Research Center for Complex Material Research (RCCM), Physics Institute, University of Würzburg, Am Hubland, D-97074 Würzburg, Germany

PACS numbers: 84.40.Ba, 73.20.Mf, 02.60.-x, 78.67.Bf

S1: QUASI-NORMAL MODES

The electric and magnetic field distributions $\tilde{\mathbf{E}}_\nu$ and $\tilde{\mathbf{H}}_\nu$ of a quasi-normal mode (QNM) can be retrieved directly from a suitably apodized FDTD simulation [1]. According to [2] a normalization factor N_ν can be calculated based on $\tilde{\mathbf{E}}_\nu$ and $\tilde{\mathbf{H}}_\nu$ which corresponds to the total energy contained within the mode fields:

$$N_\nu = \frac{1}{2}\int \left[\tilde{\mathbf{E}}_\nu \cdot \frac{\partial(\omega\varepsilon)}{\partial\omega}\tilde{\mathbf{E}}_\nu - \tilde{\mathbf{H}}_\nu \cdot \frac{\partial(\omega\mu)}{\partial\omega}\tilde{\mathbf{H}}_\nu\right] \mathrm{d}^3\mathbf{r}\,. \quad (1)$$

This allows us to normalize the electric mode field intensity to the energy contained within the QNM:

$$\mathbf{I}_\nu = \frac{|\tilde{\mathbf{E}}_\nu|^2}{N_\nu}\,, \quad (2)$$

which has the unit $\mathrm{V}^2/(\mathrm{m}^2\mathrm{eV})$. Additionally the magnetic fields have to be normalized by the same factor.

Fig. A1 shows the logarithm of the absolute values of I_ν of (a) the mode-matching antenna and (b) the reference antenna, normalized to contain the energy of 1 eV. To calculate the derivative $\partial[\omega\cdot\varepsilon(\omega)]/\partial\omega$ the data of gold modeled as in [3] have been used.

S2: DIPOLE IN FRONT OF SPHERE

To validate equation (6) from the main paper:

$$\frac{P}{P_0} = 1 + \frac{6\pi c\varepsilon_0}{k^4}\int_{V_\nu} |\mathbf{E}_p(\mathbf{r}')\cdot\mathbf{j}_\nu(\mathbf{r}')|\ \mathrm{d}^3r'\,, \quad (3)$$

we consider the problem of a dipole in front of a sphere with radius R. This case has been treated analytically by Kerker [4] and Ruppin [5] based on Mie theory [6]. Later a generalized expression for the emission power enhancement for a dipole close to a small spheres was derived based on the sphere's polarizability [7], which we will reproduce here.

We start by expressing the mode current in terms of the spheres mode fields:

$$\mathbf{j}_\nu = \sigma\mathbf{E}_\nu = i\omega\varepsilon_0(\varepsilon(\omega)-1)\mathbf{E}_\nu\,. \quad (4)$$

Inserting eq. (4) into eq. (3) then leads to:

$$\frac{P}{P_0} = 1 + \frac{6\pi\varepsilon_0^2}{k^3}\cdot \cdot \mathrm{Im}\left\{(\varepsilon(\omega)-1)\int_{V_\nu} |\mathbf{E}_p(\mathbf{r}')\cdot\mathbf{E}_\nu(\mathbf{r}')|\ \mathrm{d}^3r'\right\}. \quad (5)$$

The dipole fields inside the sphere volume can be expanded into Mie modes:

$$\mathbf{E}_\mathrm{p}(\mathbf{r},\omega) = \sum_\nu D_\nu\left[p_\nu\mathbf{M}_\nu^{(1)}(k\mathbf{r}) + q_\nu\mathbf{N}_\nu^{(1)}(k\mathbf{r})\right] \quad (6)$$

$\mathbf{M}_\nu^{(1)}$ and $\mathbf{N}_\nu^{(1)}$ are the spherical vector wave functions, as defined in [8] for a given set of control variables $\nu = n, m, \sigma$ with $n\in\mathbb{N}, m\le n\in\mathbb{N}$ and σ = odd or even, $D_\nu = \xi[(2n+1)(n-m)!]/[4n(n+1)(n+m)!]$ with $\xi = 1$

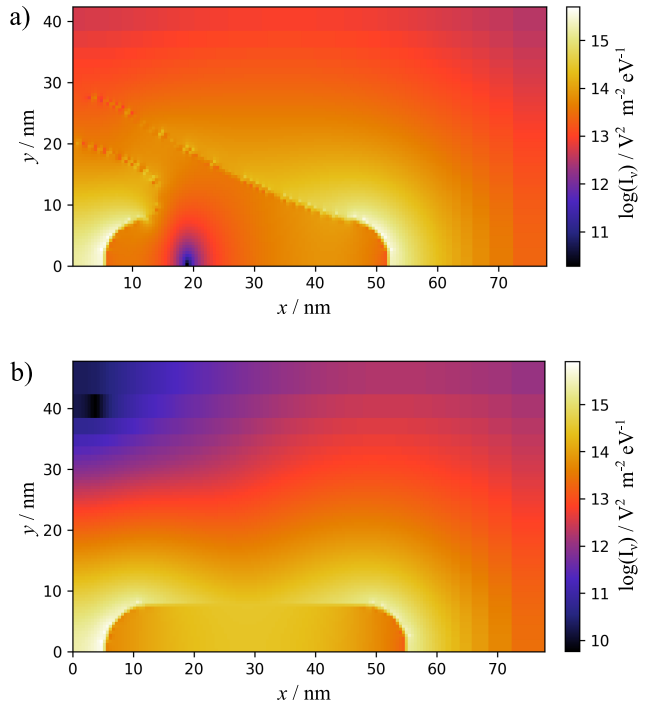

FIG. A1. Logarithm of the normalized near-field intensity I_ν in the first quadrant of the x-z-plane for (a) the best mode-matching antenna and (b) the reference antenna.

if $m = 0$ or $\xi = 2$ if $m > 0$, and

$$p_\nu = \frac{ik^3}{\varepsilon_0 \pi} \mathbf{M}_\nu^{(3)}(k\mathbf{r}_0) \cdot \mathbf{p} \tag{7}$$

$$q_\nu = \frac{ik^3}{\varepsilon_0 \pi} \mathbf{N}_\nu^{(3)}(k\mathbf{r}_0) \cdot \mathbf{p} \tag{8}$$

being prefactors originating from the Greens tensor[4].

The mode fields of the sphere read as [9]:

$$\mathbf{E}_{\mathrm{sph}}(\mathbf{r}) = \sum_\nu D_\nu \left[f_\nu \mathbf{M}_\nu^{(1)}(k_1\mathbf{r}) + g_\nu \mathbf{N}_\nu^{(1)}(k_1\mathbf{r}) \right] , \tag{9}$$

with $k_1 = k \cdot \sqrt{\varepsilon(\omega)}$, and the factors

$$f_\nu = \alpha_n p_\nu \quad ; \quad g_\nu = \beta_n q_\nu \ , \tag{10}$$

where α_n and β_n are complex valued Mie-like coefficients which are derived from the boundary conditions for electric fields at the sphere surface [5].

For a sphere with small radius and small dipole distances $R \ll r_p \ll \lambda$ we can restrict our calculation to the emission power enhancement due to the fundamental dipolar sphere mode $\mathbf{N}_{1,0,\mathrm{odd}}^{(1)} = \mathbf{N}_p$ leading to:

$$\int_{V_{\mathrm{sph}}} \mathbf{E}_p \cdot \mathbf{E}_\nu \, \mathrm{d}V = \\ = \int_{V_{\mathrm{sph}}} (D_1 q_{1,0,\mathrm{odd}} \mathbf{N}_p(k\mathbf{r})) \cdot \\ \cdot (D_1 \beta q_{1,0,\mathrm{odd}} \mathbf{N}_p(k_1\mathbf{r})) \, \mathrm{d}V \, . \tag{11}$$

Here we made use of the fact that the spherical vector wave functions are orthogonal

$$\int_{V_{\mathrm{sph}}} A_\nu \cdot B_\mu^* \, \mathrm{d}V = 0 \tag{12}$$

for $A, B \in \mathbf{N}^{(1)}, \mathbf{M}^{(1)}$ with $A \neq B$ and arbitrary ν, μ.

In the limit of small spheres the terms of the integral (11) can be developed into series of kR and kr_p respectively, which leads to the following intermediate results:

$$q_1 = \frac{ik^3}{\pi\varepsilon_0} \frac{2}{kr_p} \cdot h_1(kr_p) \tag{13}$$

$$\text{with } h_1(kr_p) = e^{ikr_p} \left(\frac{1}{kr_p} - \frac{i}{(kr_p)^2} \right) \tag{14}$$

$$\beta = \frac{3}{\varepsilon(\omega) + 2} + \mathcal{O}(k^2 R^2) \tag{15}$$

$$\int_{V_{\mathrm{sph}}} \mathbf{N}_p(k\mathbf{r}') \cdot \mathbf{N}_p(k_1\mathbf{r}') \, d^3r' = \frac{16}{27} \pi R^3 + \mathcal{O}(R^5) \tag{16}$$

with h_1 being the Hankel function of the first kind. Putting the integral together with $D_1 = 3/8$ and inserting it into eq. (5) leads to the final result:

$$\frac{P}{P_0} = 1 + \frac{3k^3}{2\pi} \cdot \\ \cdot \mathrm{Im} \left\{ \alpha_0(\omega) e^{2ikr_p} \left[\frac{1}{(kr_p)^4} - \frac{2i}{(kr_p)^5} - \frac{1}{(kr_p)^6} \right] \right\} , \tag{17}$$

which is identical to the result in [7], yet with $\alpha_0 = 4\pi R^3(\varepsilon(\omega) - 1)/(\varepsilon(\omega) + 2)$ being the quasi-static polarizability of a small sphere. Taking more terms of β into account the same result can be derived for the effective polarizability including also radiative losses [10].

S3: REVISITING THE SPLIT-RING-ANTENNA

In [11] the split-ring-antenna (sketched in Fig. A2(a)) was introduced as a result of evolutionary optimization. It has been shown that it outperforms a comparable two-wire dipolar nano antenna, reasoned by the additional current from the shortcut across the antenna gap enabling a split-ring like mode, which adds up constructively with the dipolar antenna currents for charge accumulation at the gap. Using the mode matching formalism

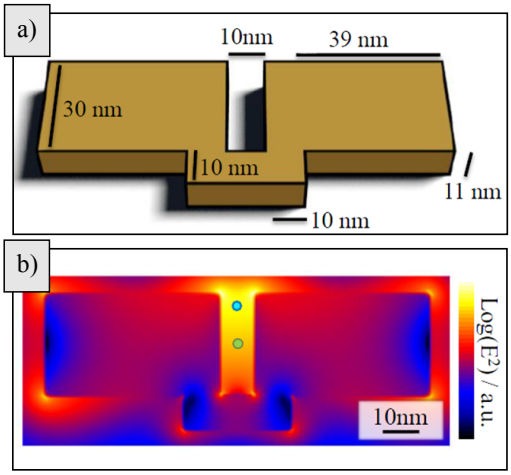

FIG. A2. (color online) Evaluation of a split-ring antenna via the mode-matching method. (a) geometry of split-ring antenna as introduced in [11]. (b) Near-field intensity distribution in the center x-y-plane. The green and blue dot represent the center of the antenna and the position of highest fields along the y-axis, respectively (more information in text).

it can now be understand, that the short cut adds a current path resembling dipolar fields in the very center of the split ring antenna.

We use this system for a numerical test of the new theory, as the SRA shows only one excitable antenna mode. We chose two positions for the dipole, one in the very center of the gap (green circle), one in the point of highest fields along the y-axis in 11 nm distance from the center (blue circle). The ratio of mode near-field at the given positions is evaluated by illuminating the antenna with a normalized Gaussian of NA= 1 and $\lambda = 650$ nm, yielding a power ratio of $P_{\mathrm{rel}} = E_{\mathrm{max}}/E_{\mathrm{center}} = 1.441$. To check the validity of eq. (3) (eq. (6) in the main paper), it is integrated numerically to obtain the mode-matching power enhancement factor P_{mm}:

$$P_{\mathrm{mm}} = \frac{P}{P_0} \propto \sum_r \mathbf{E}_\nu(r) \cdot \mathbf{E}_{\mathrm{dip}}(r) \quad . \tag{18}$$

Here r indexes all Yee-Cells within the antenna volume. The antenna has a large enough field enhancement, that direct far-field emission can be neglected. $\mathbf{E}_\nu$ was calculated with the above mentioned Gaussian excitation, the two $\mathbf{E}_{\mathrm{dip}}$ with a dipole source at a center frequency $\lambda_{\mathrm{dip}} = 650$ nm and a pulse length of ≈ 4 fs at the respective positions and a subsequent Fourier-transformation to retrieve the quasi-static fields. The ratio $P_{\mathrm{mm,max}}/P_{\mathrm{mm,center}} = 1.451$ differs from P_{rel} only by a factor of 0.007 which is within any error margin due to numerical inaccuracies for the different light source setup.

S4: GENERALIZED VERSION OF THE MODE-MATCHING FORMALISM

We reproduce eq. (1) considering a point dipole with dipole moment $\mathbf{p}$ situated at $\mathbf{r}_p$, emitting at wave number k in an inhomogeneous environment leading to scattered fields $\mathbf{E}_{\mathrm{sc}}$. The enhancement of dipole emission power P/P_0 can be calculated as [12]:

$$\frac{\gamma}{\gamma_0} = \frac{P}{P_0} = 1 + \frac{6\pi\varepsilon_0}{|\mathbf{p}|^2}\frac{1}{k^3}\mathrm{Im}\left\{\mathbf{E}_{\mathrm{sc}}(\mathbf{r}_p)\cdot\mathbf{p}^*\right\} . \tag{19}$$

Instead of eliminating the imaginary part right here, we first insert the definition of the scattered fields:

$$\mathbf{E}_{\mathrm{sc}}(\mathbf{r}_p) = i\omega\mu_0 \int_{V_\nu} \bar{\mathbf{G}}_0(\mathbf{r}_p,\mathbf{r}')\mathbf{j}_\nu(\mathbf{r}')\,\mathrm{d}^3r' , \tag{20}$$

leading together with the reciprocity theorem $\bar{\mathbf{G}}(\mathbf{r}_p,\mathbf{r}') = \bar{\mathbf{G}}(\mathbf{r}',\mathbf{r}_p)$ of the Green's tensor [13] to:

$$\frac{\gamma}{\gamma_0} = \frac{P}{P_0} = 1 + \frac{6\pi\varepsilon_0}{|\mathbf{p}|^2}\frac{\omega\mu_0}{k^3}\cdot \\ \cdot\ \mathrm{Im}\left\{\int_{V_\nu} \bar{\mathbf{G}}_0(\mathbf{r}',\mathbf{r}_p)\,\mathbf{j}_\nu(\mathbf{r}')\,\mathbf{p}^*\,\mathrm{d}^3r'\right\} . \tag{21}$$

With $\mathbf{p} = |p|\,e^{i\phi_p} \Rightarrow \mathbf{p}^* = \mathbf{p}\cdot e^{-2i\phi_p}$, the definition of the dipolar currents $j_p = -i\omega\mathbf{p}\,\delta(\mathbf{r}-\mathbf{r}_p)$ and finally applying equation (20) for the dipole fields instead, we end with:

$$\frac{P}{P_0} = 1 + \frac{6\pi c\varepsilon_0}{k^4}\cdot \\ \cdot\ \mathrm{Im}\left\{\int_{V_\nu} \mathbf{E}_p(\mathbf{r}')\cdot\mathbf{j}_\nu(\mathbf{r}')\cdot e^{-2i\phi_p}\,\mathrm{d}^3r'\right\} . \tag{22}$$

Finally we write down all phases explicitly and take again into account, that we excite the antenna at resonance with a $\pi/2$-phaseshift $\phi_\nu(\mathbf{r}) = \phi_E(\mathbf{r}) + \pi/2$. We end with:

$$\frac{P}{P_0} = 1 + \frac{6\pi c\varepsilon_0}{k^4}\cdot \\ \cdot\ \mathrm{Im}\left\{\int_{V_\nu} |\mathbf{E}_p(\mathbf{r}')|\,|\mathbf{j}_\nu(\mathbf{r}')|\cdot e^{i[2(\phi_E(\mathbf{r}')-\phi_p)+\frac{\pi}{2}]}\,\mathrm{d}^3r'\right\} , \tag{23}$$

which now also takes into account retardation effects as the extra phase term describes the self action of the dipole via the scattered fields, when the distance between dipole and antenna becomes comparable to the wavelength and $\phi_E(\mathbf{r}') - \phi_p$ remains finite.

If the antenna is excited off resonance, the phaseshift introduced before eq. (23) will no longer be $\pi/2$ but will obtain a respective value between 0 and π, which can be determined beforehand by analyzing the antenna resonance. For the case of multiple resonances the coupling terms of each resonance with respective phase enter eq. (23) via summation.

S5: N-TYPE MODE PLASMONIC CAVITY ANTENNA

To realize a plasmonic cavity antenna with cylindrical symmetry that exhibits a the n-type mode current pattern while being similar to the reference antenna, the two antenna wires have to be shortcut close to the feedpoint using a metal bridge shaped in a way that resembles the dipole field loops. To asses the optimal thickness of such a geometry we examine the approximative case of a spherical shell. Fig. A3 shows the near-field intensity enhancement in the center of spherical shells for an incoming plane wave with $\lambda = 650$ nm, while the shell radius r and shell thickness d are varied (compare also to [14]).

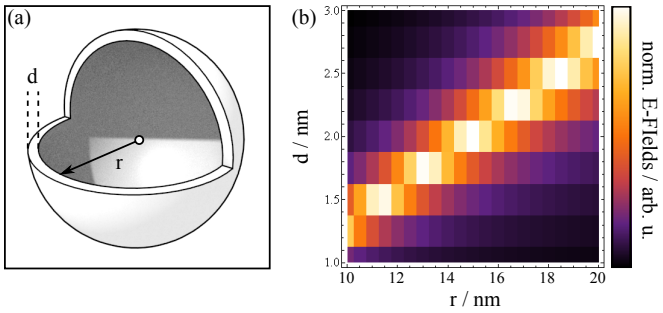

FIG. A3. Resonances of sphere shells. (a) Sketch of an air filled metal shell, with cutaway for better visibility of the dimensions r, the inner radius and d, the shell thickness. (b) Normalized electric fields in the very center (white circle) of a gold nanoshell for a quasi-static excitation at $\lambda = 650$ nm for changing shell radius and thickness.

For small shell radii with dimensions of typical optical antenna gaps, the resonant shell thickness has to be comparably thin, between 1 and 3 nm. This can be understood by an effective wavelength argument: The geometry in main paper Fig. 2(b) realizes the gap shortcut in a planar gold sheet with 30 nm thickness via two wires with a 'rectangular' cross section. To transform it to a 3D shortcut, the 'height' of the wire has to increase and its width has to shrink to keep the overall shortcut cross section area about constant to keep the identical effective plasmon wavelength and thus conserve the resonance peak position[15].

Simply combining a plasmonic dipolar antenna with a 10 nm gap with a shell with $r = 10$ nm and $d = 1$ nm (compare to Fig. A3) results in the desired mode in quasi-static FEM simulations (COMSOL). Yet, it was not possible to validate the geometry by means of full wave FDTD simulations, as down to a mesh size of 0.25 nm the stair-casing effect of the thin spherical shell leads to a severe mode shift and therefore to different NFIE spectra. Finer meshing was not feasible due to large simulation times. We note that this geometry would be of pure academic value, as a 1 nm thick, smooth spherical gold shell filled with air is far from experimental realization.

However, core-shell geometries filled with dielectric materials can be fabricated by chemical self assembly [16]. If a QE can be placed inside such a sphere, the mode-matching condition for the QE near-field can be fulfilled to a large extent. However, to achieve good far-field coupling at the same time two antenna arms have to be attached to the core-shell particles.

S6: FIELD DISTORTION AT THE AIR-GOLD INTERFACE

To prove the assumption that at optical frequencies the fields of a dipole are not strongly altered by entering a gold surface, the following figure of merit μ was devised:

$$\mu = \frac{1}{V} \int \frac{\mathbf{E}_{\mathrm{dip},0}(\mathbf{r}) \cdot \mathbf{E}_{\mathrm{dip,Au}}(\mathbf{r})}{|\mathbf{E}_{\mathrm{dip},0}(\mathbf{r})|\,|\mathbf{E}_{\mathrm{dip,Au}}(\mathbf{r})|}\,\mathrm{d}V \qquad (24)$$

The numerator in the integral is a scalar product of $\mathbf{E}_{\mathrm{dip},0}$ the dipole fields in vacuum and $\mathbf{E}_{\mathrm{dip,Au}}$ the dipole fields in gold at the same point in space $\mathbf{r}$. Together with the normalization denominator the integrand lies in the interval $[-1, 1]$, as does μ. The two fields are retrieved from two different quasistatic simulations, where the field in the gold material was retrieved from a simulation filled with gold, except of a void in the very center shaped identically to the cavity of the plasmonic cavity antenna (see Fig. 2 of the main manuscript) as depicted in Fig. A4(a). The gold materials complex dielectric $\varepsilon(\lambda) = \varepsilon'(\lambda) + i\,\varepsilon''(\lambda)$ was implemented following the Etchegoin model [3].

To define the outer border of the integration volume, an estimation for the field penetration was performed assuming the dipole fields with a r^{-3}-distance dependence being additionally damped by a factor $e^{-r/\delta(\lambda)}$ after entering the material, with δ being the penetration depth of surface plasmon fields on a plane metal/air interface [12]:

$$\delta_1(\lambda) = \frac{\lambda}{2\pi} \left(\mathrm{Im} \left(\sqrt{\frac{\varepsilon'(\lambda)^2}{\varepsilon'(\lambda) + 1}} \right) \right)^{-\frac{1}{2}} \qquad (25)$$

The resulting field decay normalized to the surface field strength for a dipole in a spherical cavity with a radius of $\lambda/100$ for wavelengths from 500 to 1000 nm in steps of 50 nm is depicted in Fig. A4(b). The minimal distance d_p between the void and the outer integration limit of eq. (24) is set to $d_p = 10$ nm, leading to an overall radius of the integrated volume of 30 nm to ensure that all fields decayed to < 0.1 of the surface field strength.

The resulting μ for a set of wavelengths λ is given in Table I. Obviously, the values are near to -1 which is expected since the fields acquire a phase shift of π on entering a metal. The absolute values are large enough

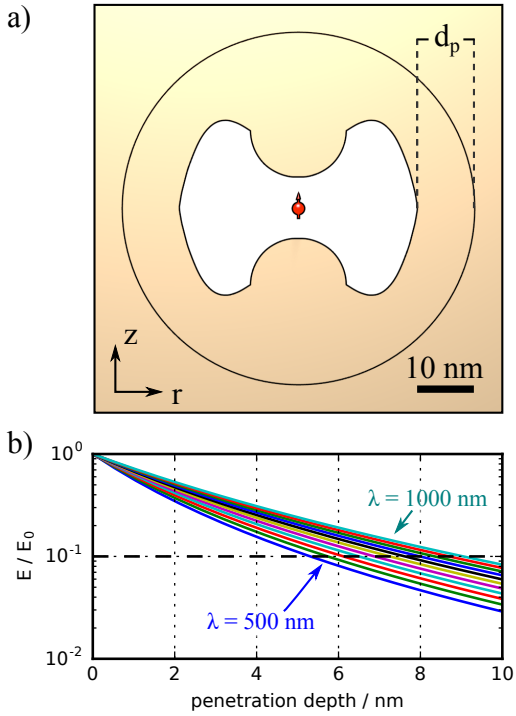

FIG. A4. (color online) The rotational symmetric geometry for the quasistatic test of field distortion. The center is filled with a single point dipole situated in the very center of the void made from vacuum. The surrounding is made from gold. The circle denotes the region, in which eq. (24) is evaluated. The minimal distance d_p was set to 10 nm (see text for details).

λ/nm	μ	μ_{Sphere}
500	0.242	-1.000
550	-0.840	-0.999
600	-0.861	-0.999
650	-0.878	-0.998
700	-0.887	-0.998
750	-0.892	-0.998
800	-0.896	-0.997
850	-0.898	-0.997
900	-0.900	-0.996
950	-0.902	-0.996
1000	-0.903	-0.996

TABLE I. Field distortion for different dipole emission wavelengths λ. μ is the value for the plasmonic cavity antenna center geometry as depicted in Fig. A4(a), while μ_{sphere} is the same calculation performed for a dipole in a spherical void (details in text).

to justify the assumption of nearly unperturbed dipole fields and the mode patterns shown in main paper Fig. 2(a) can therefore be used as design guidelines. Finally, for $\lambda = 500$ nm the absolute value of μ drops by a large margin. This is the results of the mode between the two cavity tips switching from a mode with no field node to one with two field nodes as can be seen in Fig. A5. A non-negligible portion of the field is now in phase with the excitation.

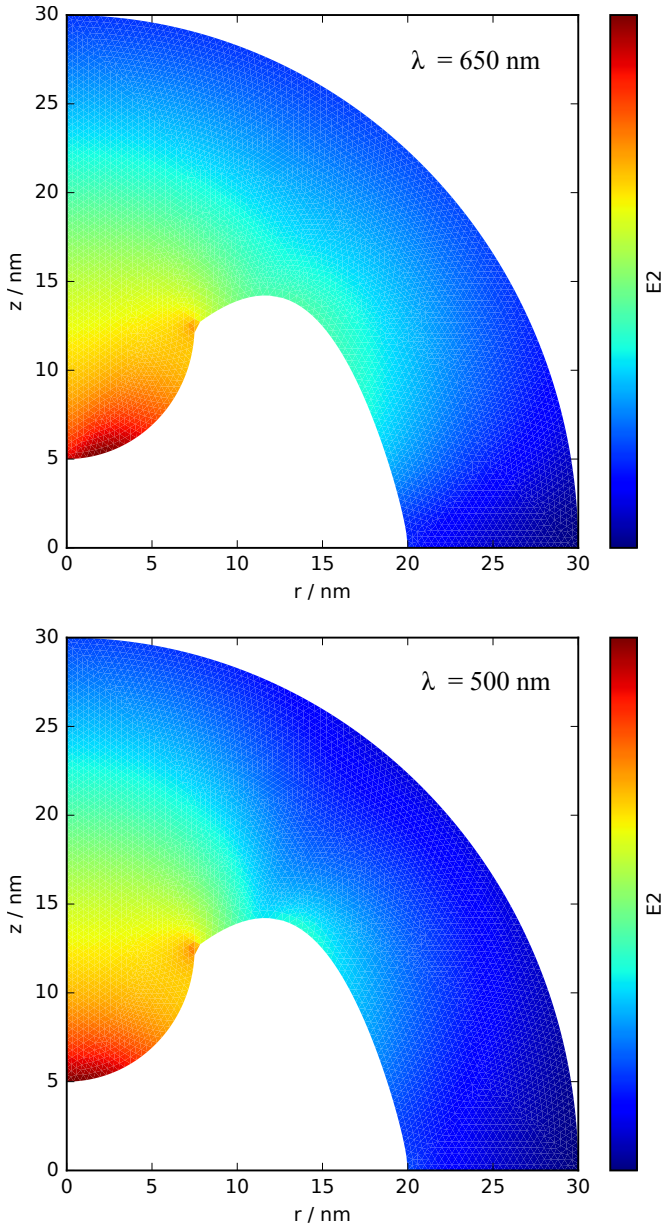

FIG. A5. Quasistatic near field intensity for $\lambda = 650$ nm (upper panel) and $\lambda = 500$ nm (lower panel) in the center region of the plasmonic cavity antenna, which was used to evaluate eq. (24). The plot shows a quarter of the cross section incorporating the axis of rotation. For $\lambda = 500$ nm an additional field strength minimum has appeared, as a higher order mode is getting excited.

It has to be mentioned, that for the cavity shape being spherical, $\mu_{\text{Sphere}} < -0.995$ is true for all examined wavelengths, when the sphere radius is set to $r = \lambda/100$ and $d_p = 10$ nm. This originates from the cavity showing the identical symmetry as the dipolar fields. However, the overlap integral and therefore the power transfer is also dependent on the field strength, which can for long

wavelengths be optimized by tips and their corresponding lightning rod effect. For short wavelengths near the plasma frequency the metallic behavior gets less and less pronounced and a spherical cavity with the lowest possible radius seems to ensure optimal coupling.

[1] C. Sauvan, J. P. Hugonin, I. S. Maksymov, and P. Lalanne, Physical Review Letters **110**, 237401 (2013).

[2] P. T. Kristensen, R.-C. Ge, and S. Hughes, Physical Review A **92**, 053810 (2015).

[3] P. G. Etchegoin, E. C. Le Ru, and M. Meyer, The Journal of Chemical Physics **125**, 164705 (2006).

[4] M. Kerker, D.-S. Wang, and H. Chew, Applied Optics **19**, 4159 (1980).

[5] R. Ruppin, The Journal of Chemical Physics **76**, 1681 (1982).

[6] G. Mie, Annalen der Physik **330**, 377445 (1908).

[7] R. Carminati, J. J. Greffet, C. Henkel, and J. M. Vigoureux, Optics Communications **261**, 368 (2006).

[8] C. F. Bohren and D. R. Huffman, *Absorption and scattering of light by small particles* (Wiley, 1983) p. 530.

[9] Ruppin[5] missed the prefactor D_ν, which is correctly included in the work of Kerker[4].

[10] W. T. Doyle, Physical Review B **39**, 9852 (1989).

[11] T. Feichtner, O. Selig, M. Kiunke, and B. Hecht, Physical Review Letters **109**, 127701 (2012).

[12] B. Hecht and L. Novotny, *Principles of Nano-Optics*, 2nd ed. (Cambridge, 2012).

[13] J. Schwinger, L. L. J. Deraad, and K. A. Milton, *Classical Electrodynamics - Chpt. 12* (Westview Press, 1998) p. 592.

[14] J. Enderlein, Applied Physics Letters **80**, 315 (2002).

[15] L. Novotny, Physical Review Letters **98**, 266802 (2007).

[16] S. A. Kalele, S. W. Gosavi, J. J. Urban, and S. K. Kulkarni, Current Science **91**, 1038 (2006).